Lithuanian Journal of Physics, Vol. **62**, No. 4, pp. 292–298 (2022)

ELECTRICAL PROPERTIES OF LLTO THICK FILMS

E. Kazakevičius [a], A. Žalga [b], V. Kavaliukė [a], S. Daugėla [a], T. Šalkus [a], and A. Kežionis [a]

[a] *Faculty of Physics, Vilnius University, Saulėtekio 3, 10222 Vilnius, Lithuania*

[b] *Faculty of Chemistry and Geosciences, Vilnius University, Naugarduko 24, 03225 Vilnius, Lithuania*

Email: edvardas.kazakevicius@ff.vu.lt

Received 7 November 2022; accepted 8 November 2022

$Li_{0.4}La_{0.56}TiO_3$ (LLTO) lithium-ion conducting solid electrolyte has been synthesized by aqueous sol-gel synthesis method. The free standing and alumina substrate supported thick films have been prepared from the obtained powder by tape casting. The films and bulk ceramics were studied by impedance spectroscopy in the frequency range from 10 Hz to 10 GHz. The equivalent circuit modelling was implemented in order to determine the electrical parameters of LLTO films and ceramics. The free standing LLTO films grain conductivity was found to be similar to the one of ceramic sample, while the grain boundary conductivity of the free standing film was slightly higher compared to LLTO ceramics.

Keywords: solid electrolyte, thick film, impedance spectroscopy, ionic conductivity

1. Introduction

Lithium-ion conducting solid materials may be applied in various electrochemical devices such as all solid state lithium batteries [1], CO_2, SO_2 or NO_2 gas sensors [2] and pH sensors [3]. $Li_{3x}La_{2/3-x}TiO_3$ (LLTO) is one of the most promising Li^+-ion solid electrolyte because of its high grain conductivity, which for $x = 0.11$ ($Li_{0.33}La_{0.56}TiO_3$) reaches the value of 0.1 S m^{-1} at room temperature [4]. LLTO crystallizes in a perovskite structure, which consists of TiO_6 octahedra and A-cages with either La^{3+} ions, Li^+ ions or vacancies surrounded by 12 oxygen ions [5, 6]. La^{3+} ions are unequally distributed in the structure forming La-rich and La-poor layers [6]. This unique superstructure leads to 2D conductivity up to 200 K [7, 8]. Such structural feature makes LLTO compound a very interesting material both for fundamental studies and for applications. However, even the high density LLTO ceramic materials have major drawback, namely the low grain boundary conductivity, which lowers the overall conductivity [9]. The LLTO ceramics are studied well and recent results are summarized in the review paper [10]. There were some attempts to prepare LLTO thin films by pulsed laser deposition [11–13], electron-beam evaporation [14] and radiofrequency magnetron sputtering [15]. Thick LLTO films were also prepared by using the tape casting method, but the conductivity value was found to be low ($\sigma_{bulk} = 1.7 \cdot 10^{-5}$ S m^{-1} @ 300 K) due to high film porosity [16]. Explicit investigation of technological tape casting conditions was performed [17] and the films with high relative density (about 98%) were prepared. The latter paper was showing electrical properties of the films at room temperature only. The conductivity values for the films were found slightly lower compared to the conductivity of ceramic samples [17]. In our present work, we have prepared free-standing LLTO films by tape casting. Our aim was a detailed investigation of electrical properties of these films. Ultrabroadband (from 10 Hz up to 10 GHz) impedance spectroscopy was used and the results were analyzed by choosing a meaningful equivalent circuit. The conductivity results of thick films were compared to the ones of bulk ceramics.

2. Experiment

The aqueous sol–gel synthesis method was used for the LLTO ceramics powder preparation. The synthesis and sintering conditions were reported previously [18]. The Li loss during the sintering is known to be a common issue [9, 11], so the lithium excess was added to provide $Li_{0.4}La_{0.56}TiO_3$ instead of $Li_{0.33}La_{0.56}TiO_3$

(the abbreviation LLTO persists through the article). The bulk ceramic samples were ground to a cylindrical shape with dimensions of l = 1.5 mm length and A = 1.0 mm^2 electrode surface area. The thick films were prepared according to the already tested tape casting methodology [16]. The 40% volume slurry was gained by mixing the powder with acetylacetone, polymethyl-methacrylate and Triton X-100 in a centrifugal mixer (Thinky ARE-250). The slurry was casted on alumina substrate with *MTI* AFA-III coater to yield the thickness of 0.2 mm after drying. Part of the film was removed from the substrate to stay free-standing. The films were measured in the 'in-plane' geometry by applying electrodes to the opposite fracture surfaces (the l and A of the film's samples are known). The Pt paste was used to prepare electrodes for impedance investigations and in both cases the paste was annealed at 1170 K for 15 min. A coaxial line with the sample was measured [19] and the impedances of the samples $\tilde{Z}(\omega) = Z'(\omega) + iZ''(\omega)$ were obtained in the frequency range ($f = \omega/2\pi$) from 10 to 10^{10} Hz and temperature range from 300 to 1000 K.

3. Results and discussion

The XRD result in relative units (Fig. 1) shows that the obtained LLTO powder has a cubic perovskite-type superstructure and is consistent with the structure No. 155633 from the ICSD database. No impurities have been observed.

The SEM micrographs of bulk ceramic sample, free standing film and alumina substrate supported film are presented in Fig. 2. All the images show well crystallized microstructures with average grain size of 2 μm and relativity high uniformity of grain size. There are no significant microstructure differences among all three samples, which allows us to compare their electrical properties.

Figure 3 shows impedance and complex capacitance spectra measured at temperatures 300, 500 and 700 K of the LLTO ceramic sample, free standing thick film and substrate supported thick film. Three dispersion regions can be seen for all the investigated samples. A dispersion region can be identified as Z' decrease with increasing frequency and the onset of the dispersion is observed as a maximum of $Z''(f)$, located at relaxation frequency. The maxima of Z'' and the dispersion region in the $Z'(f)$ representation shift towards higher frequencies when the temperature of the sample is increased. It is well known for ceramic LLTO that the impedance at the highest frequencies correspond to Li^+-ion migration in grains (Fig. 3, the maxima of $Z''(f)$ indicated as G), the midrange frequency dispersion is caused by ionic transport in grain boundaries (Fig. 3, the maxima of $Z''(f)$ indicated as GB), and the lowest frequency range dispersion is due to processes taking place at the interface of LLTO and Pt electrode (Fig. 3, the region of $Z''(f)$ indicated as E). The DC resistances of grain and grain boundary mediums (R_g and R_{gb}, respectively) can be estimated from characteristic plato regions in the spectra of $Z'(f)$ (Fig. 3, the regions of $Z'(f)$ indicated as G and GB, respectively). We have found that the impedance spectra are similar for the ceramic sample and free standing LLTO thick film, while the Z' platos and corresponding relaxation frequencies for the substrate supported thick film were shifted due to the influence of alumina substrate. The moderate shifts are

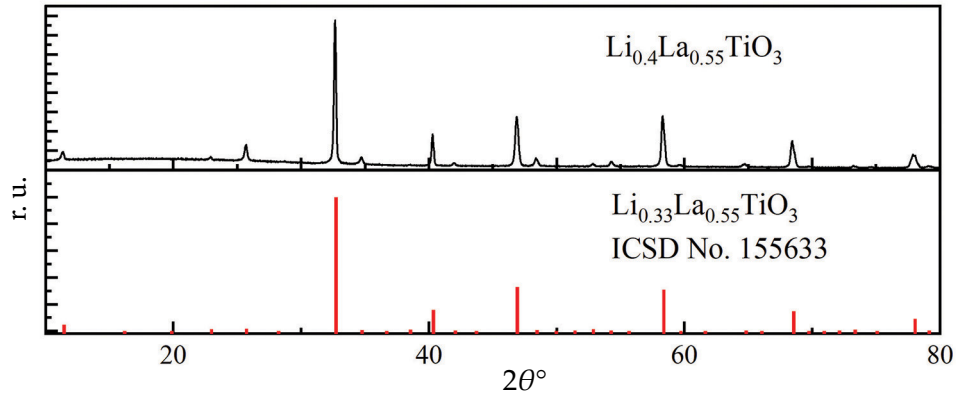

Fig. 1. XRD pattern of LLTO powder. Comparison with the data from the ICSD database is shown at the bottom.

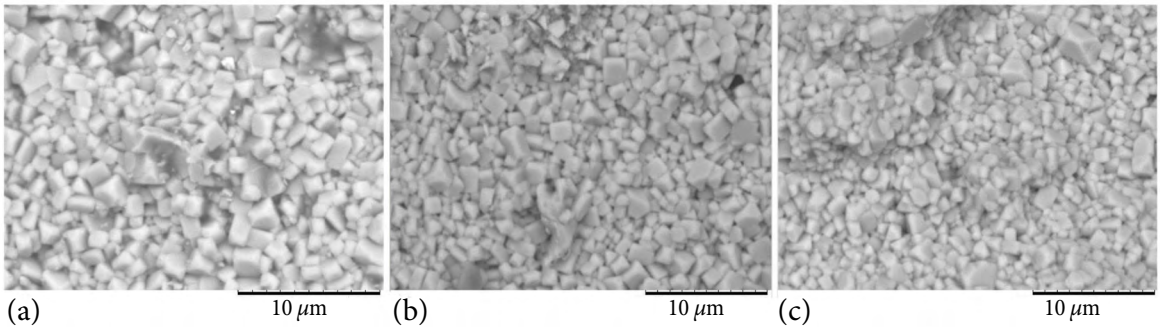

Fig. 2. SEM images of LLTO ceramics (a), free standing film (b) and alumina supported film (c).

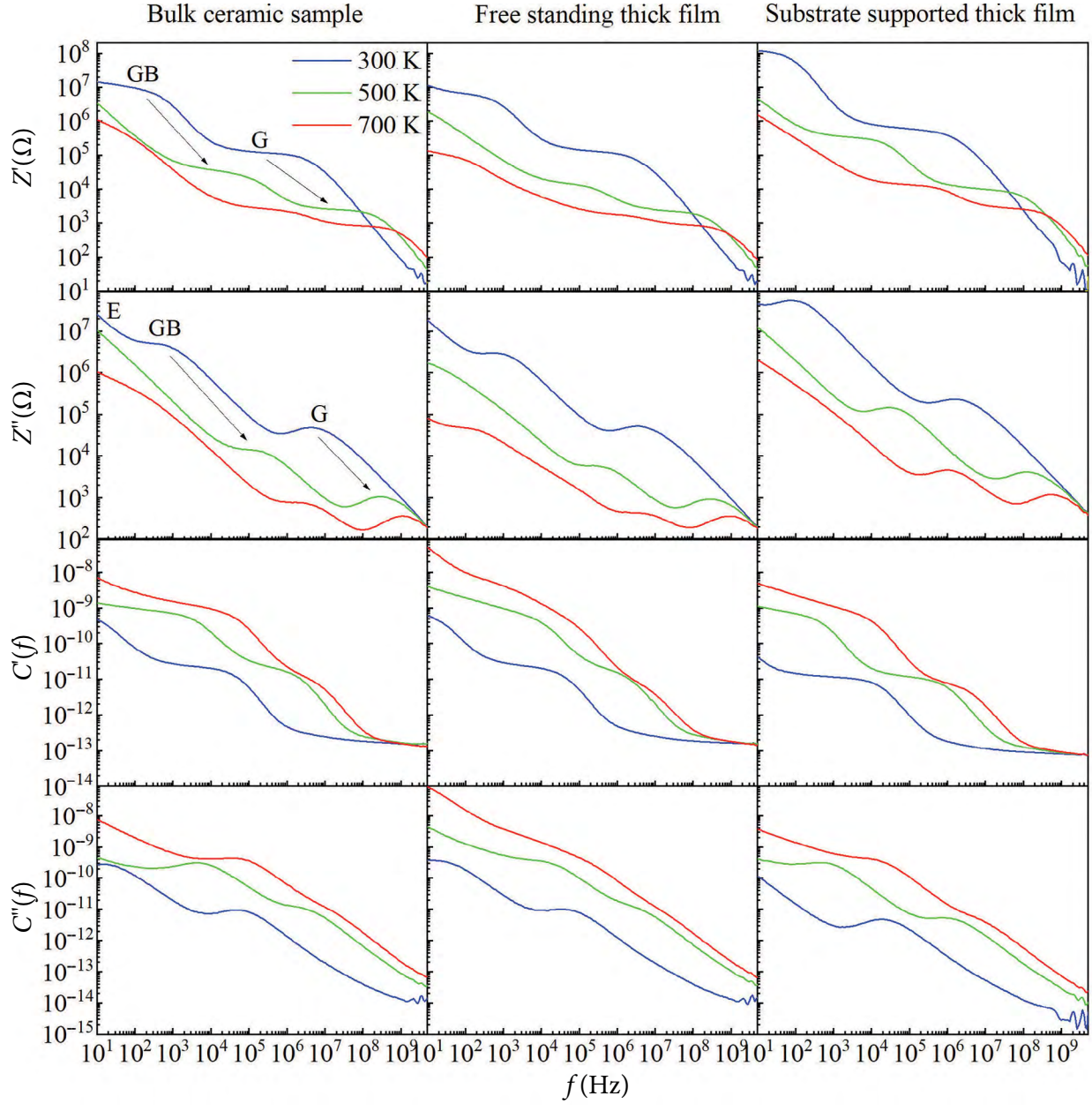

Fig. 3. Impedance and complex capacitance spectra of the LLTO bulk ceramics, free standing film and alumina supported film measured at different temperatures: 300, 500 and 700 K. The arrows indicate the shift of grain and grain boundary related spectral regions with the temperature.

also observed in the cpectra of complex capacitance $\tilde{C}(f) = C'(f) + iC''(f) = 1/(i2\pi f\tilde{Z}(f))$ due to capacitance of the substrate (Fig. 3).

The spectra differences are even more pronounced in the linear impedance spectra representation, which is shown as Nyquist plot in Fig. 4. In the Nyquist plot the diameter of the high frequency semicircle (inset of Fig. 4) corresponds to the resistance of ceramics or film grains R_g and the diameter of the semicircle in the intermediate frequency range corresponds to grain boundary resistance R_{gb}.

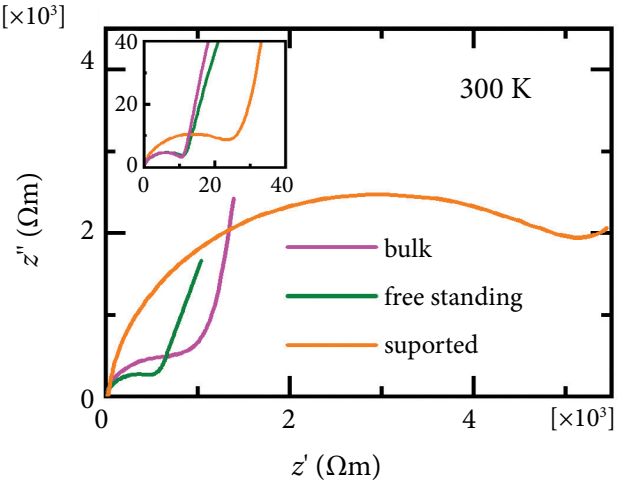

Fig. 4. Nyquist specific impedance plot of the LLTO bulk ceramics, free standing film and alumina supported film measured at 300 K. Inset shows the magnified area of the spectra at high frequencies. For fair comparison the scale is in Ωm, i.e. the impedance values are normalized to the size of the sample and denoted as z' and z''.

In order to extract sample resistances R_g and R_{gb} from the impedance spectra, the corresponding equivalent circuits have been composed. Figure 5(a) shows the equivalent circuit used to describe impedance spectra of LLTO bulk ceramics and free standing film. It is common to use a so-called ZARC circuit to describe an impedance of ionic conductors [20–22]. It consists of resistance R and constant phase element CPE [20, 23] in parallel. The impedance of the ZARC can be expressed by Eq. (1). The Q and n in Eq. (1) are parameters of CPE, the n may assume values $0 \leqslant n \leqslant 1$.

$$\tilde{Z}(\quad) = \frac{R}{1 + RQ(\mathrm{i}\quad)^n}. \tag{1}$$

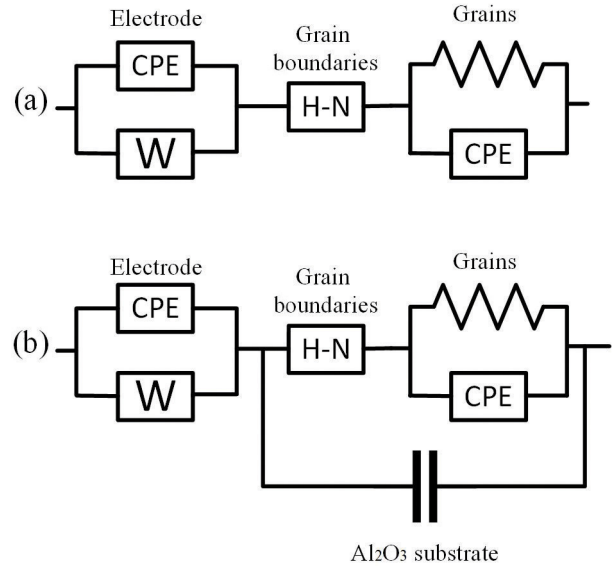

Fig. 5. Equivalent circuits used to fit the impedance spectra of LLTO ceramics and free standing film (a) and alumina supported film (b).

The $\tilde{Z}(\omega)$ of the grains were satisfactorily fitted to ZARC (indicated as 'grains' in Fig. 5(a), and describes the region G in Fig. 3) and the values of R_g were extracted. The ZARC function did not work for the impedance of grain boundaries due to strong overlap with responses E and G on both sides (Fig. 3). To get the better quality of the fit, the more generalized version of ZARC impedance, known as empirical function of Havriliak–Negami [24–27], was used (eq. (2)).

$$\tilde{Z}(\omega) = \frac{R}{\left[1 + RQ(\mathrm{i}\omega^n)\right]^m}. \tag{2}$$

The exponents in Eq. (2) may assume values such that $0 \leqslant n \times m \leqslant 1$. The representation of Havriliak–Negami function is shown as H-N element in Fig. 5(a). It describes the region GB in Fig. 3 and yields the values of R_{gb}. The common combination of CPE and Warburg [28] elements in parallel was used to fit the impedance of the electrode interface (region E in Fig. 3, Warburg element is indicated as W in Fig. 5). The equivalent circuit shown in Fig. 5(b) takes into account the alumina substrate (capacitance connected in parallel) and it was used to fit the experimental impedance spectra of substrate supported LLTO film.

Figure 6 shows the temperature dependences of grain conductivity in Arrhenius representation.

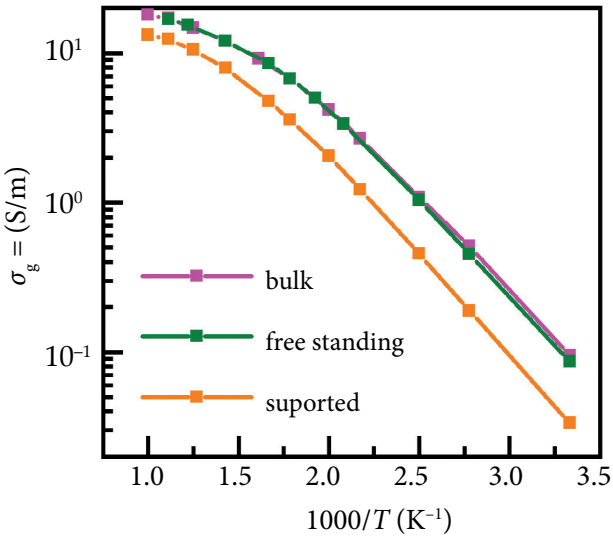

Fig. 6. Temperature dependences of the grain conductivity of bulk ceramics, free standing film and alumina supported film.

The conductivity was calculated from R_g considering the sample size, i.e. $\sigma_g = l/(AR_g)$. At high temperatures the deviation from Arrhenius law ($\sigma T = \sigma_0 \exp(\Delta E/k_B T)$) is observed. Such behaviour of LLTO bulk conductivity has already been explained by correlated Li^+-ion motion [18]. Our present results show that a similar deviation from Arrhenius activation is observed in thick LLTO films,

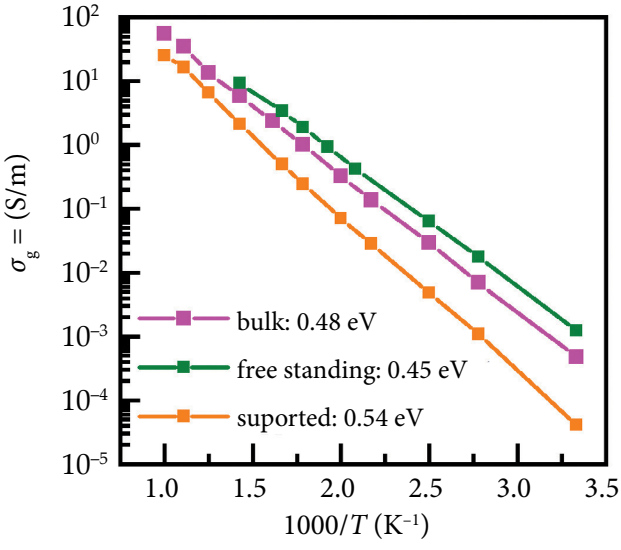

Fig. 7. Temperature dependences of the grain boundary conductivity of bulk ceramics, free standing film and alumina supported film. Conductivity activation energies were calculated after performing Arrhenius fits and are presented in eV.

both free standing and alumina supported. Besides, the grain conductivity of free standing films was almost identical with the grain conductivity of ceramics. The grain conductivity of the supported film was found to be lower: we relate this with alteration of the composition of the film due to interaction with the substrate during the sintering.

The grain boundary conductivity σ_{gb} (Fig. 7) followed Arrhenius law in the whole investigated temperature range. It is important to note that the highest value of grain boundary conductivity was found for the free standing LLTO film and its activation energy was the lowest. This suggests that the grains of the powder accommodate slightly better in the slurry than during the pressing of the dry powder.

4. Conclusions

Relatively dense LLTO thick films have been successfully tape-casted. Free standing and alumina supported films were analyzed by impedance spectroscopy in the frequency range from 10 Hz up to 10 GHz and temperatures up to 1000 K. The meaningful equivalent circuits are proposed for the analysis of impedance spectra of thick films, both free standing and supported by dielectric substrate. These equivalent circuits allowed us to extract grain and grain boundary conductivity values of the films and to compare them with the ones of bulk ceramics. In this work, we show that by using the tape-casting methodology it is possible to make free standing LLTO thick films, which show grain conductivity values identical to the bulk ceramics and even higher grain boundary conductivity values. Thus LLTO is a strong candidate for the applications where Li^+-ion solid conductors are required.

References

[1] C. Masquelier, Solid electrolytes: Lithium ions on the fast track, Nat. Mater. **10**, 649–650 (2011).

[2] G. Jasinski, P. Jasinski, A. Nowakowski, and B. Chachulski, Properties of a lithium solid electrolyte gas sensor based on reaction kinetics, Meas. Sci. Technol. **17**, 17–21 (2006).

[3] C. Bohnke, H. Duroy, and J.L. Fourquet, pH sensors with lithium lanthanum titanate sensitive material: applications in food industry, Sens. Actuators B Chem. **89**, 240–247 (2003).

[4] S. Stramare, V. Thangadurai, and W. Weppner, Lithium lanthanum titanates: A review, Chem. Mater. **15**(21), 3974–3990 (2003).

[5] J.L. Fourquet, H. Duroy, and M.P. Crosnier-Lopez, Structural and microstructural studies of the series $La_{2/3-x}Li_{3x\square 1/3-2x}TiO_3$, J. Solid State Chem. **127**, 283–294 (1996).

[6] O. Bohnke, The fast lithium-ion conducting oxides $Li_{3x}La_{2/3-x}TiO_3$ from fundamentals to application, Solid State Ion. **179**, 9–15 (2008).

[7] J. Emery, O. Bohnké, J.L. Fourquet, J.Y. Buzaré, P. Florian, and D. Massiot, Nuclear magnetic resonance investigation of Li^+-ion dynamics in the perovskite fast-ion conductor $(Li_{3x}La_{2/3-x\square 1/3-2x})TiO_3$, J. Phys. Condens. Matter **14**, 523–539 (2002).

[8] O. Bohnke, J. Emery, and J.L. Fourquet, Anomalies in Li+ ion dynamics observed by impedance spectroscopy and 7Li NMR in the perovskite fast ion conductor $(Li_{3x}La_{2/3-x\square 1/3-2x})TiO_3$, Solid State Ion. **158**(1–2), 119–132 (2003).

[9] C.W. Ban and G.M. Choi, The effect of sintering on the grain boundary conductivity of lithium lanthanum titanates, Solid State Ion. **140**, 285–292 (2001).

[10] Y. Sun, P. Guan, Y. Liu, H. Xu, S. Li, and D. Chu, Recent progress in lithium lanthanum titanate electrolyte towards all solid-state lithium ion secondary battery, Crit. Rev. Solid State Mater. Sci. **44**(4), 265–282 (2019).

[11] F. Aguesse, V. Roddatis, J. Roqueta, P. García, D. Pergolesi, J. Santiso, and J.A. Kilner, Microstructure and ionic conductivity of LLTO thin films: Influence of different substrates and excess lithium in the target, Solid State Ion. **272**, 1–8 (2015).

[12] J.K. Ahn and S.G. Yoon, Characteristics of perovskite $(Li_{0.5}La_{0.5})TiO_3$ solid electrolyte thin films grown by pulsed laser deposition for rechargeable lithium microbattery, Electrochim. Acta **50**(2–3), 371–374.

[13] O. Maqueda, F. Sauvage, L. Laffont, M.L. Martínez-Sarrión, L. Mestres, and E. Baudrin, Structural, microstructural and transport properties study of lanthanum lithium titanium perovskite thin films grown by Pulsed Laser Deposition, Thin Solid Films **516**, 1651–1655 (2008).

[14] C.L. Li, B. Zhang, and Z.W. Fu, Physical and electrochemical characterization of amorphous lithium lanthanum titanate solid electrolyte thin-film fabricated by e-beam evaporation, Thin Solid Films, **515**, 1886–1892 (2006).

[15] Y. Xiong, H. Tao, J. Zhao, H. Cheng, and X. Zhao, Effects of annealing temperature on structure and opt-electric properties of ion-conducting LLTO thin films prepared by RF magnetron sputtering, J. Alloys Compd. **509**, 1910–1914 (2011).

[16] R. Jiménez, A. del Campo, M.L. Calzada, J. Sanz, S.D. Kobylianska, S.O. Solopan, and A.G. Belous, Lithium $La_{0.57}Li_{0.33}TiO_3$ perovskite and $Li_{1.3}Al_{0.3}Ti_{1.7}(PO_4)_3$ Li–NASICON supported thick films electrolytes prepared by tape casting method, J. Electrochem. Soc. **163**, A1653–A1659 (2016).

[17] F. Schröckert, N. Schiffmann, E.C. Bucharsky, K.G. Schell, and M.J. Hoffmann, Tape casted thin films of solid electrolyte Lithium-Lanthanum-Titanate, Solid State Ion. **328**, 25–29 (2018).

[18] A. Kežionis, E. Kazakevičius, S. Kazlauskas, and A. Žalga, Metal-like temperature dependent conductivity in fast Li^+ ionic conductor Lithium Lanthanum Titanate, Solid State Ion. **342**, 115050 (2019).

[19] A. Kezionis, S. Kazlauskas, D. Petrulionis, and A.F. Orliukas, Broadband method for the determination of small sample's electrical and dielectric properties at high temperatures, IEEE Trans. Microw. Theory Tech. **62**(10), 2456–2461 (2014).

[20] J.R. Sandifer and R.P. Buck, Impedance characteristics of ion selective glass electrodes, J. Anal. Chem. **56**, 385–398 (1974).

[21] J.R. Macdonald, New aspects of some small-signal ac frequency response functions, Solid State Ion. **15**, 159–161 (1985).

[22] R.L. Hurt and J.R. Macdonald, Distributed circuit elements in impedance spectroscopy: A unified treatment of conductive and dielectric systems, Solid State Ion. **20**, 111–124 (1986).

[23] J.R. Macdonald, Note on the parameterization of the constant-phase admittance element, Solid State Ion. **13**, 147–149 (1984).

[24] S. Havriliak and S. Negami, A complex plane analysis of α-dispersions in some polymer systems, J Polym. Sci. Pol. Sym. **14**(1), 99–117 (1966).

[25] J.C. Wang and J.B. Bates, Non-Debye dielectric response and distribution of activation energies, Solid State Ion. **50**, 75–86 (1992).

[26] J.R. Macdonald and J.C. Wang, The response of systems with exponential distributions of activation energies for two classes of material temperature behavior, Solid State Ion. **60**, 319–333 (1993).

[27] J.R. Dygas, Dielectric function of ionic conductors studied by impedance spectroscopy, Solid State Ion. **176**(2), 2065–2078 (2005).

[28] A.J. Bard and L.R. Faulkner, *Electrochemical Methods, Fundamentals and Applications*, 2nd ed. (Wiley, 2000).

LLTO STORŲJŲ SLUOKSNIŲ ELEKTRINĖS SAVYBĖS

E. Kazakevičius [a], A. Žalga [b], V. Kavaliukė [a], S. Daugėla [a], T. Šalkus [a], A. Kežionis [a]

[a] *Vilniaus universiteto Fizikos fakultetas, Vilnius, Lietuva*

[b] *Vilniaus universiteto Chemijos ir geomokslų fakultetas, Vilnius, Lietuva*

Santrauka

$Li_{0,4}La_{0,56}TiO_3$ (LLTO) ličio jonų laidininkai buvo sintezuoti zolių-gelių metodu. Rentgeno spindulių difrakcijos analizė parodė, kad šis junginys kristalizuodamasis sudaro perovskito struktūrą, o kitų priemaišinių fazių stebėta nebuvo. Iš gautų superjoninių miltelių sluoksnių liejimo metodu buvo pagaminti stori sluoksniai: vienas ant aliuminio oksido padėklo, kitas – be padėklo. LLTO keramika ir storieji sluoksniai buvo ištirti pilnutinės varžos spektroskopijos metodu dažnių srityje tarp 10 Hz ir 10 GHz. Rezultatams nagrinėti buvo pasitelkta ekvivalentinių grandinių analizė. Nustatyta, kad LLTO sluoksnio be padėklo kristalinis laidumas yra identiškas keramikos kristaliniam laidumui, o tarpkristalinis šio sluoksnio laidumas gautas kiek didesnis, palyginti su to paties junginio keramika.